Volume 9 No 2 December (2026)

e-ISSN: 2615-3270
p-ISSN: 2615-3599

Eigen Mathematics Journal

Homepage Journal: https://eigen.unram.ac.id/index.php/eigen

Adaptive Sliding Mode Control for Vaccination and Treatment in a Measles Transmission Model

Dewi Suhika[1*], Rifky Fauzi[1], Nela Rizka[1], Achmad Suryadi Nasution[1], Mira Mustika[1], Werry Febrianti[1], Dear Michiko Mutiara Noor[1], Lutfi Mardianto[1]

[1] *Mathematics Study Program, Institut Teknologi Sumatera, Indonesia*
[*] *Corresponding author: dewi.suhika@ma.itera.ac.id*

A B S T R A C T

Measles remains a highly contagious vaccine-preventable disease, and persistent outbreaks highlight the need for effective intervention strategies combining prevention and treatment. This study develops an extended measles transmission model consisting of susceptible, vaccinated, exposed, infectious, hospitalized, and recovered populations, with two time-dependent control inputs representing vaccination and treatment. An Adaptive Sliding Mode Control (ASMC) strategy is proposed to regulate the vaccinated population toward a prescribed trajectory while suppressing the infectious population. Normalized sliding surfaces are constructed for the vaccinated and infectious states, and adaptive gains incorporating a dead-zone mechanism are introduced to prevent unnecessary gain growth. The positivity and boundedness of the epidemiological model solutions are established, while Lyapunov analysis demonstrates exponential convergence of the ideal sliding dynamics when the control saturation constraints are inactive. Numerical simulations are conducted over 200 weeks with an initial population of 10 million individuals, comparing the proposed ASMC strategy with an uncontrolled scenario under the same initial conditions and epidemiological parameters. The uncontrolled infectious population reaches a peak of approximately 364,005 individuals, whereas under ASMC it does not exceed its initial value of 75,900, corresponding to a 79.15% reduction in the peak infectious population relative to the uncontrolled scenario. At the end of the simulation, the vaccinated population reaches approximately 4.61×10^6 individuals, representing 46.09% of the modeled population. Moreover, the control inputs and adaptive gains remain bounded throughout the numerical simulation. These findings illustrate the potential of the proposed ASMC framework for coordinating vaccination and treatment interventions and reducing the simulated peak infectious population.

Keywords: Measles, Adaptive sliding mode control, Vaccination, Treatment, Epidemic control

Received : 03-09-2026;
Revised : 15-10-2026;
Accepted : 10-11-2026;
Published : 25-11-2026;

DOI: https://doi.org/10.29303/emj.v9i2.481

This work is licensed under a CC BY-NC-SA 4.0 International license

1. Introduction

Measles is a highly contagious vaccine-preventable disease caused by the measles virus of the genus Morbillivirus. The disease is primarily transmitted through respiratory droplets and airborne exposure from infectious individuals and remains a significant public health concern despite the availability of

effective vaccines [1, 2]. Vaccination is the principal strategy for preventing measles transmission by reducing the susceptible population and increasing population-level immunity. However, insufficient vaccination coverage may create immunity gaps that allow sustained transmission and recurrent outbreaks [3, 4]. This challenge remains particularly relevant in Indonesia, where a substantial resurgence of measles has recently been reported. In 2025, the Ministry of Health of the Republic of Indonesia reported 11,094 confirmed measles cases and 63,769 suspected cases, representing a 147% increase compared with 2024, with 69 associated deaths [5, 6]. Infants under one year of age accounted for approximately 68% of the reported cases, indicating the continuing vulnerability of populations with incomplete or absent immunization [5]. Moreover, recent reports indicate that a substantial proportion of measles cases occurred among unvaccinated individuals, highlighting persistent gaps in immunization coverage [5, 6]. These epidemiological conditions emphasize the importance of strengthening vaccination programs while simultaneously implementing appropriate management and treatment of infectious individuals to reduce the burden of infection and limit further transmission.

Mathematical modeling provides a useful framework for describing measles transmission dynamics and evaluating the potential effects of different intervention strategies. Various compartmental models have been proposed to investigate the roles of vaccination, treatment, and hospitalization in measles transmission [7–9]. In the Indonesian context, Abadi et al. [7] developed an SIHR model incorporating vaccination and hospitalization and applied the model to recorded measles data from Jakarta in 2017. Their analysis demonstrated that hospitalization of infectious individuals could complement vaccination in reducing measles transmission. This study provides an important basis for investigating the interaction between preventive and therapeutic interventions in measles dynamics. However, intervention mechanisms in conventional compartmental models are commonly represented by fixed parameters or prescribed intervention rates. Such formulations are useful for epidemiological analysis, but they do not necessarily provide a feedback mechanism capable of dynamically adjusting intervention intensity in response to changes in the disease states.

This limitation motivates the incorporation of control-theoretic approaches into epidemiological models. Sliding Mode Control (SMC) is a robust nonlinear control approach that has been widely investigated for systems subject to uncertainties and disturbances [10, 11]. Its robustness makes it attractive for epidemiological systems whose parameters and disease states may be subject to uncertainty [10]. In epidemic control problems, SMC can be used to dynamically regulate intervention inputs, such as vaccination, isolation, or treatment, in order to drive selected epidemiological states toward desired levels and suppress disease transmission [12–15]. Nevertheless, conventional SMC generally requires an appropriate switching gain to be specified in advance. An insufficient gain may compromise the reaching condition, whereas an excessively large gain may increase control effort and aggravate chattering. Adaptive sliding mode control (ASMC) alleviates this requirement by allowing the switching gain to evolve according to the system trajectory or sliding variable [16, 17]. In epidemiological applications, this adaptive mechanism enables the control intensity to respond to changes in disease dynamics, providing stronger intervention when the deviation from the desired epidemiological state is large and reducing unnecessary control effort when the system approaches its target [17]. However, adaptation laws based only on the magnitude of the sliding variable may cause the adaptive gain to continue increasing when residual tracking errors persist. To address this issue, a dead-zone adaptation mechanism can be introduced, allowing the adaptive gain to increase when the sliding variable exceeds a prescribed threshold and to remain constant when the sliding variable enters the dead-zone. This mechanism prevents unnecessary gain accumulation when the tracking error becomes sufficiently small.

In comparison with previous studies, Abadi et al. [7] investigated measles transmission using an SIHR model incorporating vaccination and hospitalization. Meanwhile, Aldila et al. [18] developed an optimal control framework based on Pontryagin's Maximum Principle (PMP) to evaluate vaccination and quarantine strategies. In contrast, the present study employs an SVEIHR model with two feedback control inputs representing vaccination and treatment. While the PMP-based approach determines intervention strategies through the optimization of an objective functional, the proposed ASMC framework determines feedback control inputs based on sliding surfaces constructed from prescribed vaccination and infectious population trajectories. Furthermore, the adaptive gains incorporate a dead-zone mechanism to prevent unnecessary gain accumulation when the tracking errors become sufficiently small. These differences highlight the methodological contribution of the proposed framework in terms of dual reference tracking and adaptive feedback control.

Motivated by these considerations, this study develops an adaptive control framework for a measles transmission model consisting of susceptible, vaccinated, exposed, infectious, hospitalized, and recovered populations. The model incorporates two time-dependent control inputs representing vaccination and treatment interventions. Unlike epidemiological modeling approaches that primarily analyze disease dynamics under prescribed intervention rates, the proposed framework introduces feedback control laws that dynamically adjust vaccination and treatment efforts based on the system states.

The main methodological contribution of this study is the development of a two-input adaptive sliding mode control framework with a dead-zone adaptation mechanism for simultaneously regulating vaccination and infectious disease dynamics. Two normalized sliding surfaces are constructed from the tracking errors of the vaccinated and infectious populations. Unlike conventional SMC with predetermined switching gains, the proposed adaptive mechanism allows the gains to increase when the sliding variables exceed a prescribed dead-zone threshold and to remain constant once the tracking errors enter the dead-zone. This approach prevents unnecessary gain accumulation while maintaining adaptive control action during transient tracking. Furthermore, the control inputs are constrained by prescribed admissible bounds, and the stability properties of the ideal sliding dynamics are investigated using Lyapunov analysis under inactive control saturation.

Accordingly, the objective of this study is to develop and evaluate an adaptive sliding mode control strategy for coordinating vaccination and treatment interventions in measles transmission dynamics. The proposed controller is designed to increase the vaccinated population toward a desired vaccination trajectory while simultaneously reducing the infectious population toward a prescribed reference level. The mathematical properties of the controlled model and the convergence behavior of the proposed controller are investigated, followed by numerical simulations comparing the controlled and uncontrolled dynamics. Controller performance is examined through reference tracking, convergence of the sliding surfaces, evolution of the adaptive gains, behavior of the constrained control inputs, and the simulated reduction in the peak infectious population.

2. Mathematical Model and Control Design

This section presents the mathematical formulation and fundamental properties of the proposed measles transmission model as the basis for the subsequent control design. The population compartments, transmission mechanisms, and intervention inputs are first formulated, followed by an analysis of the positivity and boundedness of the model solutions. These properties ensure the epidemiological feasibility of the model before the adaptive sliding mode control strategy is developed.

2.1. Mathematical Model Formulation

The measles transmission model considered in this study is developed based on the epidemiological framework proposed by Abadi et al. [7], with several modifications introduced to accommodate

the objectives of the present study. In particular, the model is extended by explicitly incorporating vaccinated and exposed populations and by introducing vaccination and treatment as time-dependent control interventions. Accordingly, the total population is divided into six epidemiological compartments: susceptible individuals $S(t)$, vaccinated individuals $V(t)$, exposed individuals $E(t)$, infectious individuals $I(t)$, hospitalized individuals $H(t)$, and recovered individuals $R(t)$. The total population at time t is therefore given by

$$N(t) = S(t) + V(t) + E(t) + I(t) + H(t) + R(t). \tag{1}$$

The inclusion of the vaccinated and exposed compartments allows the model to explicitly represent vaccination dynamics and the latent stage of measles infection before individuals become infectious. Two time-dependent control inputs are incorporated into the model, namely $u_1(t)$, representing vaccination applied to susceptible individuals, and $u_2(t)$, representing treatment applied to infectious individuals.

The model is formulated under several epidemiological and mathematical assumptions. First, the population is assumed to be homogeneously mixed, such that individuals have equal opportunities for contact with infectious individuals. This assumption simplifies the transmission process by neglecting heterogeneity in age, spatial distribution, and contact patterns, as commonly considered in compartmental epidemic models [19]. Disease transmission occurs through contact with individuals in the infectious compartment, while exposed individuals are assumed to be infected but not yet infectious. Second, vaccination is assumed to provide partial protection against infection, represented by the vaccine efficacy parameter ϵ. This assumption is consistent with previous measles modeling studies that account for imperfect vaccine protection [18]. Third, vaccine-induced protection is assumed to wane over time, allowing vaccinated individuals to return to the susceptible compartment. Previous research has investigated the effects of waning vaccine-derived immunity on measles transmission [?]. However, the use of a constant waning rate in the present model is adopted as a mathematical simplification rather than a direct representation of heterogeneous immunity durations. Fourth, infectious individuals may recover naturally, receive treatment, or be hospitalized, whereas hospitalized individuals may subsequently recover. Recruitment is included in the population dynamics, and natural mortality is assumed to occur at the same per capita rate μ across all compartments, consistent with common assumptions in compartmental measles models [7]. Disease-induced mortality and migration are not explicitly considered. Thus, homogeneous mixing, constant waning and transition rates, and uniform natural mortality are primarily adopted for mathematical tractability, whereas partial vaccine protection and the possibility of waning immunity are motivated by epidemiological considerations.

Susceptible individuals enter the population at a recruitment rate Λ and may acquire measles infection through effective contact with infectious individuals at the transmission rate β, resulting in the force of infection $\beta I/N$. Susceptible individuals are transferred to the vaccinated compartment through the vaccination control $u_1(t)$. Vaccinated individuals are assumed to receive partial protection against infection, characterized by the vaccine efficacy parameter ϵ, where $0 \leq \epsilon \leq 1$. Consequently, breakthrough infection among vaccinated individuals occurs at the reduced rate $(1-\epsilon)\beta VI/N$. Vaccine-induced protection may wane at rate ω, resulting in the return of vaccinated individuals to the susceptible compartment.

Individuals who acquire infection enter the exposed compartment $E(t)$, where they are infected but not yet infectious. Exposed individuals progress to the infectious compartment at rate σ. Infectious individuals may recover naturally at rate γ_1, be hospitalized at rate δ, or receive treatment through the control input $u_2(t)$. The treatment intervention is assumed to increase the removal of infectious individuals from the infectious compartment and transfer them directly to the recovered compart-

ment. Hospitalized individuals recover at rate γ_2. Natural mortality occurs in all epidemiological compartments at rate μ.

The transmission dynamics of the proposed measles model are illustrated in Figure 1. The arrows represent transitions between epidemiological compartments due to recruitment, infection, vaccination, disease progression, hospitalization, treatment, recovery, waning vaccine-induced protection, and natural mortality. In particular, the control input $u_1(t)$ regulates the transition from the susceptible to the vaccinated compartment, whereas $u_2(t)$ regulates the treatment-induced transition from the infectious to the recovered compartment.

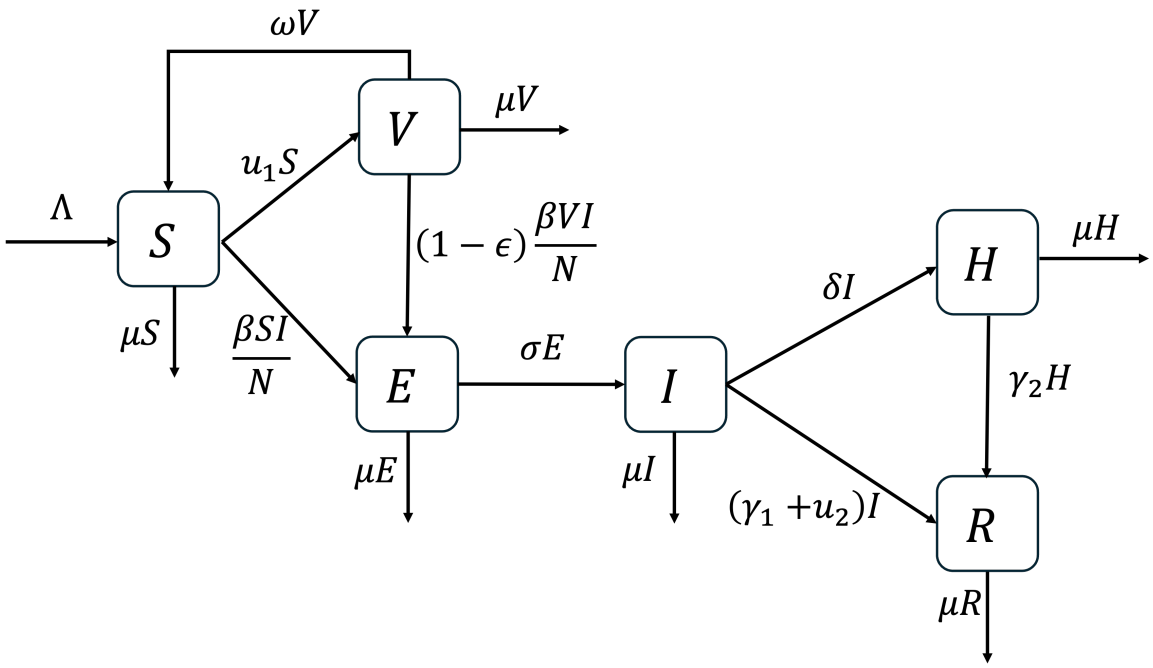

Figure 1. Transmission diagram of the proposed measles model.

Based on the transmission processes illustrated in Figure 1, the dynamics of the proposed measles model are governed by the following system of nonlinear ordinary differential equations:

$$\begin{aligned}
\frac{dS}{dt} &= \Lambda - \frac{\beta SI}{N} - u_1(t)S - \mu S + \omega V,\\
\frac{dV}{dt} &= u_1(t)S - (1-\epsilon)\frac{\beta VI}{N} - (\omega+\mu)V,\\
\frac{dE}{dt} &= \frac{\beta SI}{N} + (1-\epsilon)\frac{\beta VI}{N} - (\sigma+\mu)E,\\
\frac{dI}{dt} &= \sigma E - (\delta+\gamma_1+\mu+u_2(t))\,I,\\
\frac{dH}{dt} &= \delta I - (\gamma_2+\mu)H,\\
\frac{dR}{dt} &= (\gamma_1+u_2(t))\,I + \gamma_2 H - \mu R.
\end{aligned} \tag{2}$$

The control input $u_1(t)$ represents the vaccination intensity applied to susceptible individuals, whereas $u_2(t)$ represents the treatment intensity applied to infectious individuals. The admissible

control inputs are assumed to satisfy

$$0 \le u_1(t) \le u_{1,\max}, \qquad 0 \le u_2(t) \le u_{2,\max}, \tag{3}$$

where $u_{1,\max}$ and $u_{2,\max}$ denote the maximum admissible vaccination and treatment intensities, respectively. These bounds ensure that the control actions remain nonnegative and within feasible intervention levels.

The state variables and parameters involved in system (2) are summarized in Tables 1 and 2, respectively.

Table 1. State variables of the measles transmission model.

Variable	Description
$S(t)$	Susceptible individuals
$V(t)$	Vaccinated individuals
$E(t)$	Exposed individuals
$I(t)$	Infectious individuals
$H(t)$	Hospitalized individuals
$R(t)$	Recovered individuals

Throughout this study, time is measured in weeks. Accordingly, all epidemiological rate parameters are expressed in units of week^{-1}. The recruitment rate Λ is expressed in individuals per week, while vaccine efficacy ϵ is dimensionless. The numerical simulations are conducted over a period of 200 weeks.

Table 2. Parameters of the measles transmission model.

Parameter	Description	Value	Unit	Source
Λ	Recruitment rate	μN_0	individuals/week	Assumed
β	Measles transmission rate	0.4984	week^{-1}	[7]
ϵ	Vaccine efficacy	0.95	dimensionless	[18]
σ	Progression rate from exposed to infectious	1.00	week^{-1}	[18]
δ	Hospitalization rate of infectious individuals	0.000165	week^{-1}	[7]
γ_1	Recovery rate of infectious individuals	0.3333	week^{-1}	[7]
γ_2	Recovery rate of hospitalized individuals	1.00	week^{-1}	[7]
μ	Natural mortality rate	$\frac{1}{72.67 \times 53}$	week^{-1}	[18]
ω	Rate of waning vaccine-induced protection	$\frac{1}{20 \times 52}$	week^{-1}	[19]

The epidemiological interpretation of system (2) follows directly from the transitions illustrated in Figure 1. Recruitment increases the susceptible population, whereas infection, vaccination, and natural mortality reduce it. Vaccination transfers susceptible individuals to the vaccinated compartment, while waning vaccine-induced protection returns vaccinated individuals to the susceptible compartment. Both susceptible and vaccinated individuals may become exposed following effective contact with infectious individuals; however, the infection rate among vaccinated individuals is reduced by the factor $1 - \epsilon$. Exposed individuals progress to the infectious compartment at rate σ. Infectious individuals may recover naturally at rate γ_1, be hospitalized at rate δ, or receive treatment through $u_2(t)$, which transfers them to the recovered compartment. Hospitalized individuals subsequently recover at rate γ_2.

Summing all equations in system (2) gives the total population dynamics

$$\frac{dN}{dt} = \Lambda - \mu N. \tag{4}$$

All internal transitions associated with infection, vaccination, treatment, hospitalization, recovery, and waning vaccine-induced protection cancel in the total population balance. The solution of (4) is

$$N(t) = \frac{\Lambda}{\mu} + \left(N_0 - \frac{\Lambda}{\mu}\right) e^{-\mu t}, \tag{5}$$

where $N_0 = N(0)$ denotes the initial total population. Therefore, $N(t)$ remains bounded and approaches Λ/μ as t increases. In the numerical simulations, the recruitment rate is chosen as

$$\Lambda = \mu N_0, \tag{6}$$

so that $N(t) = N_0$ and the total population remains constant throughout the simulation.

For the subsequent control design, the main epidemiological objectives are to increase vaccination coverage and suppress the infectious population. Accordingly, $V(t)$ and $I(t)$ are selected as the controlled states. Desired reference trajectories $V_d(t)$ and $I_d(t)$ are introduced to describe the intended evolution of the vaccinated and infectious populations, respectively. These reference trajectories are subsequently used to construct the sliding surfaces and develop the adaptive sliding mode control strategy.

2.2. Positivity and Boundedness of Solutions

Before developing the control strategy, it is necessary to establish that the proposed measles model is epidemiologically well posed. In particular, all state variables must remain non-negative for non-negative initial conditions, and the total population must remain bounded for all $t \geq 0$.

Theorem 2.1. *If $S(0), V(0), E(0), I(0), H(0), R(0) \geq 0$, all epidemiological parameters are non-negative, and the control inputs satisfy (3), then every solution of system (2) remains non-negative for all $t \geq 0$.*

Proof. The positivity of the solutions can be established by examining the vector field on the boundary of the non-negative orthant. For $S = 0$, the first equation of system (2) gives

$$\left.\frac{dS}{dt}\right|_{S=0} = \Lambda + \omega V \geq 0.$$

For $V = 0$,

$$\left.\frac{dV}{dt}\right|_{V=0} = u_1(t) S \geq 0.$$

Similarly, for $E = 0$,

$$\left.\frac{dE}{dt}\right|_{E=0} = \frac{\beta S I}{N} + (1-\epsilon)\frac{\beta V I}{N} \geq 0.$$

For $I = 0$,

$$\left.\frac{dI}{dt}\right|_{I=0} = \sigma E \geq 0.$$

For $H = 0$,

$$\left.\frac{dH}{dt}\right|_{H=0} = \delta I \geq 0.$$

For $R = 0$,

$$\left.\frac{dR}{dt}\right|_{R=0} = [\gamma_1 + u_2(t)]\, I + \gamma_2 H \geq 0.$$

Therefore, the vector field points inward or is tangent to the boundary of the non-negative orthant. Consequently, none of the state variables can cross from a non-negative value into the negative region. Hence,

$$S(t), V(t), E(t), I(t), H(t), R(t) \geq 0, \qquad t \geq 0.$$

We next establish the strict positivity of the susceptible and infectious populations for strictly positive initial values. From the susceptible population equation, we have

$$\frac{dS}{dt} = \Lambda + \omega V - \left(\frac{\beta I}{N} + u_1 + \mu\right) S.$$

Since $\Lambda + \omega V \geq 0$, it follows that

$$\frac{dS}{dt} \geq -\left(\frac{\beta I}{N} + u_1 + \mu\right) S.$$

By the comparison principle,

$$S(t) \geq S(0) \exp\left(-\int_0^t \left[\frac{\beta I(\tau)}{N(\tau)} + u_1(\tau) + \mu\right] d\tau\right) > 0,$$

provided that $S(0) > 0$.

Similarly, the infectious population equation satisfies

$$\frac{dI}{dt} = \sigma E - (\delta + \gamma_1 + \mu + u_2) I.$$

Since $\sigma E \geq 0$, we obtain

$$\frac{dI}{dt} \geq -(\delta + \gamma_1 + \mu + u_2) I.$$

Applying the comparison principle gives

$$I(t) \geq I(0) \exp\left(-\int_0^t [\delta + \gamma_1 + \mu + u_2(\tau)] d\tau\right) > 0,$$

whenever $I(0) > 0$.

Thus, $S(t)$ and $I(t)$ remain strictly positive for every finite time under bounded admissible controls. In particular, the denominators appearing in the analytical vaccination and treatment control laws remain nonzero for strictly positive initial susceptible and infectious populations. □

Theorem 2.2. *Let $N(t) = S(t) + V(t) + E(t) + I(t) + H(t) + R(t)$, and assume that $\mu > 0$ and $N(0) > 0$. Then every solution of system (2) with non-negative initial conditions is bounded. In particular,*

$$N(t) = \frac{\Lambda}{\mu} + \left(N(0) - \frac{\Lambda}{\mu}\right) e^{-\mu t},$$

and therefore

$$N(t) \leq \max\left\{N(0), \frac{\Lambda}{\mu}\right\}, \qquad t \geq 0.$$

Proof. Adding all equations in system (2) yields

$$\frac{dN}{dt} = \Lambda - \mu N.$$

The infection, vaccination, treatment, hospitalization, recovery, and waning-immunity terms cancel because they represent internal transfers between epidemiological compartments. Solving the resulting differential equation gives

$$N(t) = \frac{\Lambda}{\mu} + \left(N(0) - \frac{\Lambda}{\mu}\right) e^{-\mu t}.$$

Since $0 < e^{-\mu t} \leq 1$ for $t \geq 0$ and $\mu > 0$, it follows that

$$N(t) \leq \max\left\{N(0), \frac{\Lambda}{\mu}\right\}.$$

Moreover, since $N(0) > 0$ and $\Lambda \geq 0$, the explicit solution implies that $N(t) > 0$ for every finite $t \geq 0$.

Thus, the total population remains bounded for all $t \geq 0$. Consequently, the biologically feasible region

$$\Omega = \left\{(S, V, E, I, H, R) \in \mathbb{R}^6_+ : S + V + E + I + H + R \leq M\right\}$$

where

$$M = \max\left\{N(0), \frac{\Lambda}{\mu}\right\}$$

is positively invariant under the dynamics of (2). □

3. Results and Discussion

This section presents the design and numerical evaluation of the proposed Adaptive Sliding Mode Control (ASMC) strategy for the measles transmission model. The analysis includes the formulation of the controller, comparison of the controlled and uncontrolled transmission dynamics, evaluation of the vaccinated and infectious tracking performance, and examination of the sliding surfaces and adaptive gains. The main findings and limitations of the proposed framework are also discussed.

3.1. Adaptive Sliding Mode Control Design

The proposed adaptive sliding mode control strategy is designed to achieve two epidemiological objectives, namely increasing the vaccinated population and suppressing the infectious population. To represent these objectives, desired reference trajectories are introduced for the vaccinated and infectious populations.

Definition 3.1. *Let $V_d(t)$ denote the desired trajectory of the vaccinated population and $I_d(t)$ denote the desired trajectory of the infectious population. The reference trajectories are defined as*

$$V_d(t) = V_0 + (V_{\max} - V_0)\left(1 - e^{-r_V t}\right), \tag{7}$$

and

$$I_d(t) = I_{\min} + (I_0 - I_{\min})\, e^{-r_I t}, \tag{8}$$

where $V_0 = V(0)$, $I_0 = I(0)$, $V_{\max}$ is the prescribed vaccination target, $I_{\min}$ is the prescribed minimum infectious level, and $r_V, r_I > 0$ determine the rates at which the reference trajectories approach their respective targets.

The corresponding time derivatives of the reference trajectories are

$$\dot{V}_d(t) = r_V \left(V_{\max} - V_0\right) e^{-r_V t}, \tag{9}$$

and

$$\dot{I}_d(t) = -r_I \left(I_0 - I_{\min}\right) e^{-r_I t}. \tag{10}$$

For numerical implementation, the desired vaccination and infectious levels may be expressed as proportions of the total population,

$$V_{\max} = p_V N, \qquad I_{\min} = p_I N, \tag{11}$$

where $0 < p_V < 1$ and $0 \leq p_I < 1$. The specific values of p_V, p_I, r_V, and r_I are specified in the numerical simulation section. Since the model time variable is measured in weeks, the reference trajectory rates r_V and r_I are expressed in week^{-1}. This ensures that the exponential terms in the desired vaccination and infectious trajectories are dimensionless.

To quantify the deviations of the vaccinated and infectious populations from their respective reference trajectories, normalized sliding surfaces are introduced. Normalization by the total population reduces the influence of population scale and allows the two tracking errors to be evaluated on comparable scales.

Definition 3.2. *The normalized tracking errors associated with the vaccinated and infectious populations are defined by the sliding surfaces*

$$s_1(t) = \frac{V_d(t) - V(t)}{N}, \tag{12}$$

and

$$s_2(t) = \frac{I(t) - I_d(t)}{N}. \tag{13}$$

The condition $s_1(t) = 0$ corresponds to $V(t) = V_d(t)$, whereas $s_2(t) = 0$ corresponds to $I(t) = I_d(t)$. Assuming that the total population remains constant, differentiation of (12) gives

$$\dot{s}_1 = \frac{1}{N}\left(\dot{V}_d - \dot{V}\right). \tag{14}$$

Using the vaccinated population equation yields

$$\dot{s}_1 = \frac{1}{N}\left[\dot{V}_d - u_1 S + (1-\epsilon)\frac{\beta V I}{N} + (\omega + \mu)V\right]. \tag{15}$$

Similarly, differentiating (13) gives

$$\dot{s}_2 = \frac{1}{N}\left(\dot{I} - \dot{I}_d\right), \tag{16}$$

and therefore

$$\dot{s}_2 = \frac{1}{N}\left[\sigma E - (\delta + \gamma_1 + \mu)I - u_2 I - \dot{I}_d\right]. \tag{17}$$

The desired reaching laws are selected as

$$\dot{s}_1 = -k_1(t)s_1 - \eta_1 \operatorname{sat}\left(\frac{s_1}{\phi_1}\right), \tag{18}$$

and

$$\dot{s}_2 = -k_2(t)s_2 - \eta_2 \,\mathrm{sat}\left(\frac{s_2}{\phi_2}\right), \tag{19}$$

where $k_1(t), k_2(t) > 0$ are adaptive gains, $\eta_1, \eta_2 > 0$ are switching coefficients, and $\phi_1, \phi_2 > 0$ determine the boundary-layer thicknesses. The saturation function is defined as

$$\mathrm{sat}(z) = \begin{cases} z, & |z| \le 1, \\ \mathrm{sgn}(z), & |z| > 1. \end{cases} \tag{20}$$

Equating (15) with the desired reaching law (18) gives the vaccination control law

$$u_1^*(t) = \frac{\dot{V}_d + (1-\epsilon)\dfrac{\beta V I}{N} + (\omega+\mu)V + N\left[k_1 s_1 + \eta_1 \,\mathrm{sat}\left(\dfrac{s_1}{\phi_1}\right)\right]}{S}. \tag{21}$$

Similarly, from (17) and (19), the treatment control law is obtained as

$$u_2^*(t) = \frac{\sigma E - (\delta+\gamma_1+\mu)I - \dot{I}_d + N\left[k_2 s_2 + \eta_2 \,\mathrm{sat}\left(\dfrac{s_2}{\phi_2}\right)\right]}{I}. \tag{22}$$

To satisfy the admissible intervention bounds, the implemented controls are defined using the projection operator

$$u_1(t) = \min\left\{u_{1,\max}, \max\left\{0, u_1^*(t)\right\}\right\}, \tag{23}$$

and

$$u_2(t) = \min\left\{u_{2,\max}, \max\left\{0, u_2^*(t)\right\}\right\}. \tag{24}$$

The control inputs $u_1(t)$ and $u_2(t)$ represent vaccination and treatment rates, respectively, and are expressed in week^{-1}. Since the sliding surfaces are normalized by the total population, they are dimensionless. Accordingly, the adaptive gains $k_i(t)$ and switching coefficients η_i are expressed in week^{-1}, whereas the boundary-layer parameters ϕ_i are dimensionless. The admissible upper bounds $u_{1,\max}$ and $u_{2,\max}$ are also expressed in week^{-1}.

To prevent continuous growth of the adaptive gains in the presence of small residual tracking errors, a dead-zone adaptation mechanism is introduced.

Definition 3.3. *For $i = 1, 2$, the adaptive gain $k_i(t)$ is governed by*

$$\dot{k}_i = \begin{cases} \gamma_{a_i}(|s_i| - \varepsilon_a), & |s_i| > \varepsilon_a, \\ 0, & |s_i| \le \varepsilon_a, \end{cases} \tag{25}$$

where $\gamma_{a_i} > 0$ is the adaptation rate, $k_{i0} > 0$ is the nominal initial gain, and $\varepsilon_a > 0$ denotes the dead-zone threshold.

When the tracking error is sufficiently large, the adaptive gain increases according to the magnitude of the sliding variable exceeding the dead-zone threshold. When the sliding variable enters the dead-zone, the adaptation stops and the adaptive gain remains constant at its most recently attained value. This mechanism prevents unnecessary gain accumulation near the desired trajectories. For dimensional consistency, the adaptation coefficients γ_{a_i} are expressed in week^{-2}. The nominal gains k_{i0} have units of week^{-1}, whereas the dead-zone threshold ε_a is dimensionless.

3.1.1. Stability Analysis

The following theorem establishes the stability of the proposed sliding dynamics.

Theorem 3.4. *Consider the sliding surfaces defined by (12) and (13). Suppose that $k_i(0) = k_{i0} > 0$, $\eta_i > 0$, and $\phi_i > 0$, for $i = 1, 2$, and that the adaptive gains evolve according to (25). Assume that the unconstrained control laws (21) and (22) remain within the admissible control bounds such that the projection operators are inactive for all $t \geq 0$. Then, the sliding surfaces $s_1(t)$ and $s_2(t)$ converge exponentially to zero. Consequently, the origin of the sliding dynamics is exponentially stable under the stated conditions.*

Proof. Consider the Lyapunov candidate function

$$\mathcal{L}(s_1, s_2) = \frac{1}{2}s_1^2 + \frac{1}{2}s_2^2. \tag{26}$$

Clearly, $\mathcal{L}(s_1, s_2) \geq 0$, with $\mathcal{L}(s_1, s_2) = 0$ if and only if $s_1 = s_2 = 0$. Differentiating (26) along the system trajectories gives

$$\dot{\mathcal{L}} = s_1\dot{s}_1 + s_2\dot{s}_2. \tag{27}$$

Substituting the reaching laws (18) and (19) into (27) yields

$$\begin{aligned}\dot{\mathcal{L}} = & -k_1 s_1^2 - \eta_1 s_1 \,\mathrm{sat}\left(\frac{s_1}{\phi_1}\right) \\ & - k_2 s_2^2 - \eta_2 s_2 \,\mathrm{sat}\left(\frac{s_2}{\phi_2}\right).\end{aligned} \tag{28}$$

For any s_i, the saturation function satisfies

$$s_i \,\mathrm{sat}\left(\frac{s_i}{\phi_i}\right) \geq 0. \tag{29}$$

Indeed, if $|s_i| > \phi_i$, then

$$s_i \,\mathrm{sat}\left(\frac{s_i}{\phi_i}\right) = |s_i|,$$

whereas if $|s_i| \leq \phi_i$, then

$$s_i \,\mathrm{sat}\left(\frac{s_i}{\phi_i}\right) = \frac{s_i^2}{\phi_i}.$$

Since $k_i(t) > 0$, $\eta_i > 0$, and $\phi_i > 0$, every term on the right-hand side of (28) is nonpositive. Consequently,

$$\dot{\mathcal{L}} \leq 0. \tag{30}$$

Moreover, according to the adaptive law (25), the adaptive gains satisfy $\dot{k}_i(t) \geq 0$. Since $k_i(0) = k_{i0} > 0$, it follows that $k_i(t) \geq k_{i0}$ for all $t \geq 0$. Let $k_{\min} = \min\{k_{10}, k_{20}\} > 0$. Using (29), Equation (28) implies

$$\dot{\mathcal{L}} \leq -k_{\min}(s_1^2 + s_2^2) = -2k_{\min}\mathcal{L}. \tag{31}$$

By the comparison principle, we obtain

$$\mathcal{L}(t) \leq \mathcal{L}(0)e^{-2k_{\min}t}. \tag{32}$$

Consequently,

$$\sqrt{s_1^2(t) + s_2^2(t)} \leq \sqrt{s_1^2(0) + s_2^2(0)} e^{-k_{\min} t}. \tag{33}$$

Therefore, the sliding surfaces converge exponentially to zero, establishing exponential stability of the origin of the sliding dynamics under the stated unsaturated control conditions. Although the saturation functions introduce boundary layers to reduce chattering, they do not prevent convergence to zero in the ideal sliding dynamics considered here. □

Remark (Effect of Control Saturation). The stability result established in Theorem 3.4 applies when the unconstrained control laws (21) and (22) remain within their admissible bounds, such that the projection operators (23) and (24) are inactive. When either control input is actively saturated, the implemented control differs from its unconstrained counterpart. Consequently, the actual sliding dynamics may deviate from the prescribed reaching laws (18) and (19), and the Lyapunov inequality derived above is not automatically guaranteed. Therefore, the exponential convergence established in Theorem 3.4 is guaranteed only when the prescribed reaching laws are satisfied under the unsaturated control conditions. The numerical simulations illustrate the tracking performance of the constrained system, including intervals of active control saturation, but do not constitute a general theoretical proof of stability during these intervals.

Theorem 3.5. Suppose that the conditions of Theorem 3.4 are satisfied. Then, convergence of the sliding surfaces toward their respective boundary layers implies that the vaccinated and infectious populations approach the neighborhoods of their prescribed reference trajectories $V_d(t)$ and $I_d(t)$, respectively.

Proof. From the definition of the first sliding surface,

$$s_1(t) = \frac{V_d(t) - V(t)}{N}, \tag{34}$$

which can be rearranged as

$$V(t) - V_d(t) = -N s_1(t). \tag{35}$$

Therefore, as $s_1(t)$ approaches its boundary layer around zero, the difference between $V(t)$ and $V_d(t)$ becomes correspondingly small.

Similarly, from

$$s_2(t) = \frac{I(t) - I_d(t)}{N}, \tag{36}$$

it follows that

$$I(t) - I_d(t) = N s_2(t). \tag{37}$$

Hence, as $s_2(t)$ approaches its boundary layer around zero, the infectious population approaches the neighborhood of the desired infectious trajectory.

Consequently, the proposed controller regulates the vaccinated population toward its prescribed vaccination trajectory while simultaneously suppressing the infectious population toward the desired epidemiological reference. □

Theorem 3.6. *Consider the adaptive law (25) with $\gamma_{a_i} > 0$ and $k_i(0) = k_{i0} > 0$, for $i = 1, 2$. Suppose that the conditions of Theorem 3.4 are satisfied, so that the sliding variables converge exponentially to zero. Then, the adaptive gains remain positive, nondecreasing, and bounded. Furthermore, the adaptive gains become constant after the corresponding sliding variables enter and remain within the dead-zone.*

Proof. For $|s_i| > \varepsilon_a$, the adaptive law (25) gives

$$\dot{k}_i = \gamma_{a_i}(|s_i| - \varepsilon_a) > 0. \tag{38}$$

For $|s_i| \le \varepsilon_a$, the adaptation law reduces to

$$\dot{k}_i = 0. \tag{39}$$

Therefore, $\dot{k}_i(t) \ge 0$ for all t, implying that

$$k_i(t) \ge k_i(0) = k_{i0} > 0. \tag{40}$$

Thus, the adaptive gains remain positive and nondecreasing.

Furthermore, under the conditions of Theorem 3.4, the sliding variables satisfy the exponential convergence estimate

$$\sqrt{s_1^2(t) + s_2^2(t)} \le \sqrt{s_1^2(0) + s_2^2(0)}e^{-k_{\min}t}, \tag{41}$$

where $k_{\min} = \min\{k_{10}, k_{20}\} > 0$. Therefore, the sliding variables are bounded and converge exponentially to zero. Since $\varepsilon_a > 0$, there exists a finite time t_a such that $|s_i(t)| \le \varepsilon_a$ for all $t \ge t_a$ and $i = 1, 2$. Consequently, the adaptive law (25) gives

$$\dot{k}_i(t) = 0, \qquad t \ge t_a. \tag{42}$$

Hence,

$$k_i(t) = k_i(t_a), \qquad t \ge t_a. \tag{43}$$

Since the sliding variables are bounded, the adaptation rates are bounded on the finite interval $[0, t_a]$. Thus, the adaptive gains remain finite before t_a and constant thereafter. Therefore, the adaptive gains are bounded under the conditions of Theorem 3.4, without requiring an independent boundedness assumption on the sliding variables.

□

3.2. Numerical Simulation and Measles Dynamics under ASMC

The numerical simulations are performed over a time horizon of 200 weeks. The initial conditions are given by

$$S(0) = 9,242,000, \qquad V(0) = 500,000, \qquad E(0) = 10,000,$$
$$I(0) = 75,900, \qquad H(0) = 56, \qquad R(0) = 172,044,$$

corresponding to an initial total population of $N_0 = 10,000,000$. The recruitment rate is set as $\Lambda = \mu N_0$. The epidemiological parameter values used in the simulations are summarized in Table 2.

For the ASMC implementation, the vaccination and infectious reference trajectories are prescribed according to the reference functions introduced previously. The vaccination reference increases toward its prescribed target, whereas the infectious reference decreases toward a low infectious level. The normalized sliding surfaces are defined by

$$s_1(t) = \frac{V_d(t) - V(t)}{N}, \qquad s_2(t) = \frac{I(t) - I_d(t)}{N}.$$

The first control input $u_1(t)$ regulates vaccination, while $u_2(t)$ represents treatment applied to infectious individuals.

The ASMC parameters are set as $\gamma_{a1} = 0.05$, $\gamma_{a2} = 0.50$, $k_{10} = k_{20} = 0.10$, $\eta_1 = \eta_2 = 0.05$, and $\phi_1 = \phi_2 = 0.001$. The dead-zone threshold is $\varepsilon_a = 10^{-4}$, and the maximum adaptive gains are $k_{1,\max} = k_{2,\max} = 1.00$. The control bounds are $u_{1,\max} = 0.20$ and $u_{2,\max} = 0.50$, while the regularization parameter is $\varepsilon_I = 10^{-6}$. The adaptive gain law employs a dead-zone mechanism without leakage, with additional upper bounds imposed on the adaptive gains in the numerical implementation. The numerical solutions are obtained using MATLAB `ode45` over 200 weeks, with relative and absolute tolerances of 10^{-7} and 10^{-8}, respectively. Nonnegative constraints are imposed on the state variables.

The effects of the proposed ASMC strategy on the six epidemiological compartments are presented in Figure 2(a)–(f). As shown in Figure 2(a), the susceptible population decreases to approximately 4.72×10^6 individuals without control and 3.92×10^6 under ASMC at $t = 200$. The lower susceptible population under ASMC is associated with the transfer of susceptible individuals into the vaccinated compartment. Accordingly, Figure 2(b) shows that the vaccinated population increases from 5.0×10^5 to approximately 4.61×10^6 individuals under ASMC, corresponding to approximately 46.09% of the total population, while it decreases to approximately 3.77×10^5 without control. The controlled vaccination trajectory closely follows the prescribed reference trajectory in the numerical results.

The effects on disease progression are shown in Figure 2(c)–(e). In particular, Figure 2(d) shows that the uncontrolled infectious population increases from 75,900 to a peak of approximately 364,005 individuals at $t = 31.66$ weeks, whereas under ASMC no subsequent peak above the initial infectious level occurs. The controlled infectious peak is therefore approximately 79.15% lower than the uncontrolled peak.

The percentage reduction is calculated by comparing the peak infectious populations in the uncontrolled and controlled simulations:

$$\text{Peak reduction} = \frac{I_{\text{peak,uncontrolled}} - I_{\text{peak,ASMC}}}{I_{\text{peak,uncontrolled}}} \times 100\% = \frac{364005 - 75900}{364005} \times 100\% \approx 79.15\%. \tag{44}$$

This percentage represents the reduction in the simulated peak infectious population under the specified model assumptions and parameter settings, rather than an empirically established reduction in measles cases.

The suppression of infection is accompanied by lower exposed and hospitalized trajectories, as shown in Figure 2(c) and (e). Finally, Figure 2(f) shows a lower recovered population under ASMC, approximately 1.48×10^6 compared with 4.90×10^6 without control at $t = 200$. This difference is associated with fewer individuals passing through infection before recovery under the vaccination and treatment interventions.

3.3. Tracking and Adaptive Control Performance

The tracking and adaptive control performance is further evaluated through the reference trajectories, control inputs, sliding surfaces, and adaptive gains. The vaccination and infectious trajectories are regulated toward their prescribed references, while the corresponding control efforts are shown in Fig. 3. The vaccination control $u_1(t)$ initially reaches its upper bound $u_{1,\max} = 0.20$ and subsequently decreases as the vaccination tracking error becomes smaller. Similarly, the treatment control $u_2(t)$ initially operates at its upper bound $u_{2,\max} = 0.50$ before decreasing to zero as the infectious population is suppressed. This behavior indicates that stronger intervention is required during the initial transient period, whereas the required control effort decreases as the system approaches the desired trajectories.

It should be noted that the control inputs reach their prescribed upper bounds during the initial intervention period, indicating that the control constraints become active. During intervals of active control saturation, the implemented control inputs may differ from the unconstrained control laws,

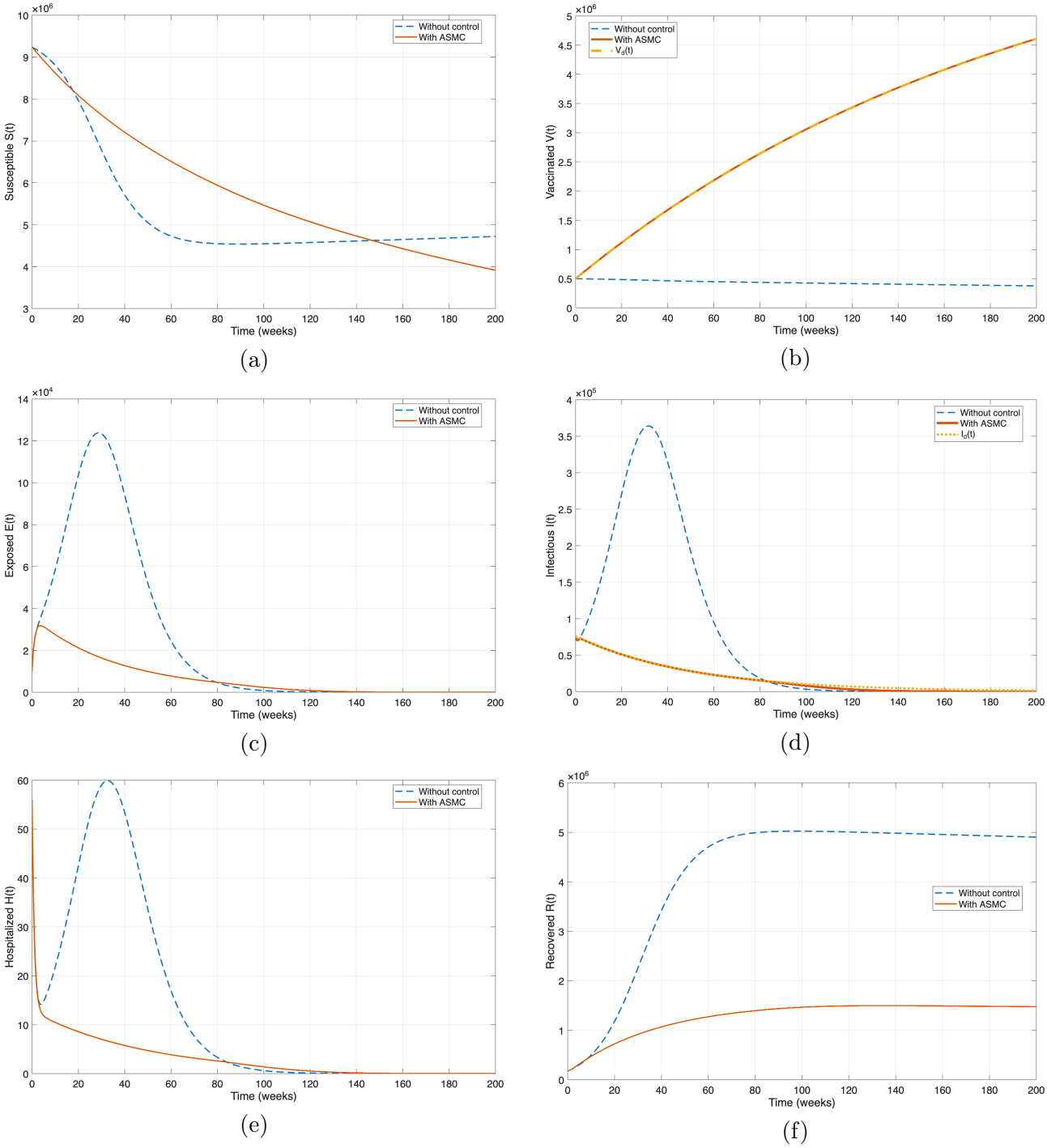

Figure 2. Comparison of measles transmission dynamics without control and under the proposed ASMC strategy: (a) susceptible, (b) vaccinated, (c) exposed, (d) infectious, (e) hospitalized, and (f) recovered populations.

and the stability result established in Theorem 3.4 does not directly apply. Therefore, although the numerical results demonstrate satisfactory tracking performance under the imposed control constraints, they should not be interpreted as a general theoretical guarantee of stability during control saturation.

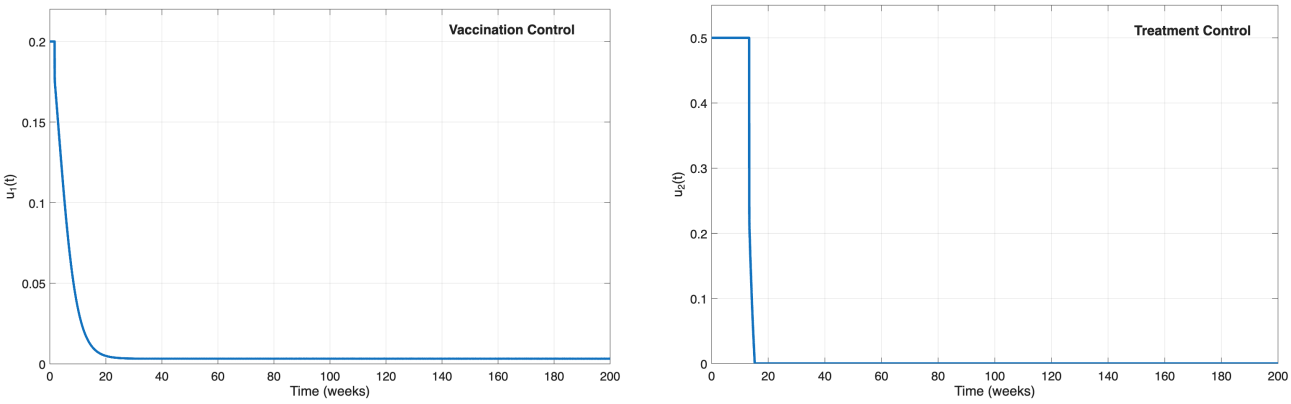

(a) (b)

Figure 3. Control inputs under the proposed ASMC strategy: (a) vaccination control $u_1(t)$ and (b) treatment control $u_2(t)$.

The convergence behavior of the tracking errors is illustrated in Fig. 4. The magnitudes of the normalized sliding surfaces, $|s_1|$ and $|s_2|$, decrease toward the prescribed dead-zone threshold ε_a and subsequently remain close to zero. The vaccination sliding surface exhibits a short initial transient before rapidly converging, whereas the infectious sliding surface decreases more gradually. These results indicate that the controlled states approach the desired tracking region and remain within a small neighborhood of their prescribed trajectories.

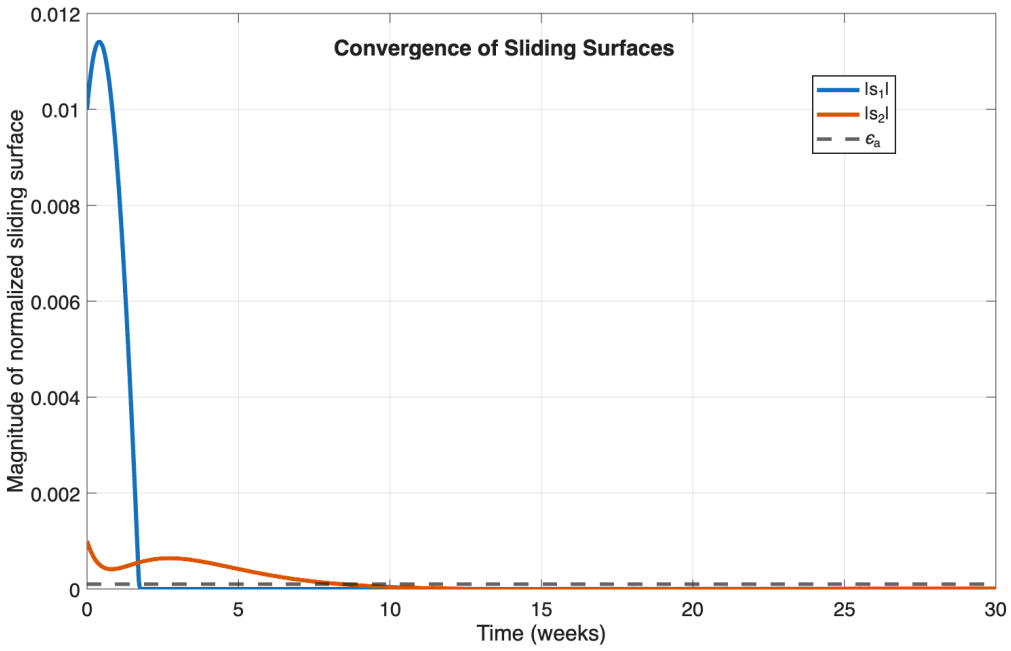

Figure 4. Convergence of the normalized sliding surface magnitudes under the proposed ASMC strategy.

The corresponding adaptive gains are presented in Fig. 5. Starting from the nominal value $k_{10} = k_{20} = 0.1$, both gains increase during the transient phase when the respective sliding-surface magnitudes remain outside the dead zone. The gain $k_1(t)$ reaches its steady value earlier because the vaccination tracking error enters the dead-zone more rapidly, whereas $k_2(t)$ adapts for a longer period in response to the infectious tracking error. Once the corresponding sliding surface enters the dead-zone, the adaptation stops and the gain remains constant. Hence, the dead-zone mechanism prevents unnecessary continuous growth of the adaptive gains.

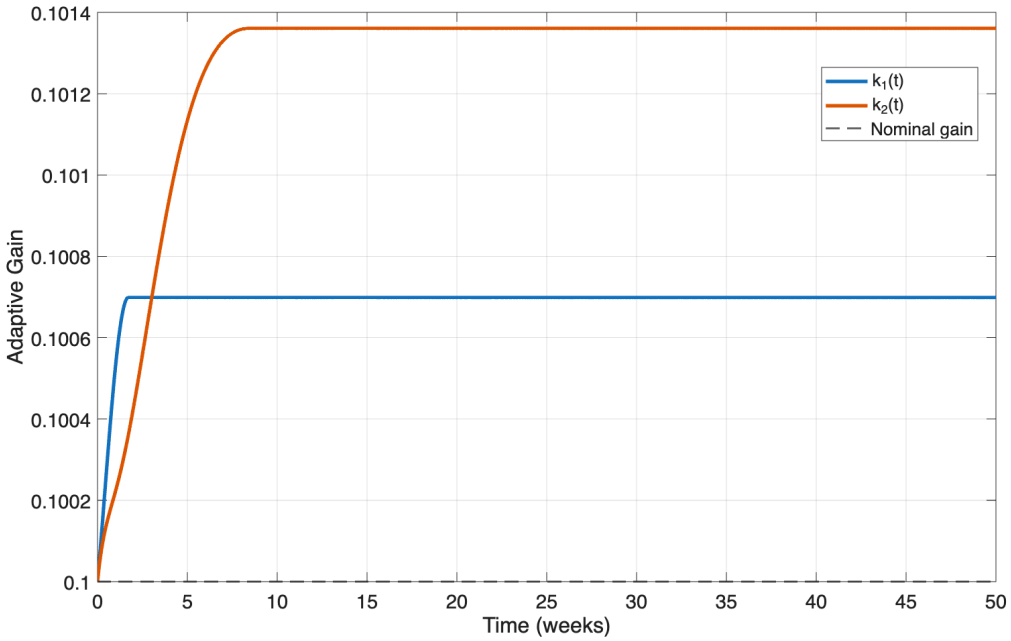

Figure 5. Evolution of the adaptive gains under the dead-zone adaptation mechanism.

The numerical results indicate that the proposed ASMC strategy effectively combines vaccination and treatment to suppress measles transmission. In particular, the controller prevents the pronounced epidemic growth observed in the uncontrolled system while increasing the vaccinated population under the prescribed control constraints. The sliding surface convergence and bounded adaptive gains further demonstrate that the controller achieves the desired response without continuous gain accumulation.

The proposed model has several limitations that should be considered when interpreting the numerical results and assessing their practical applicability. The homogeneous mixing assumption neglects differences in contact patterns among individuals, while constant epidemiological parameters do not capture temporal variations in transmission associated with seasonal effects, behavioral changes, or public health interventions. Furthermore, the absence of age-structured and spatial components limits the ability of the model to represent differences in infection risk and intervention requirements across demographic groups and geographical regions. Consequently, the reported reduction in the peak infectious population should be interpreted as a model-based numerical result under the specified assumptions and simulation conditions, rather than a direct prediction of intervention effectiveness in real-world settings. In addition, the reference trajectories and control bounds are prescribed for numerical evaluation and should not be interpreted directly as public health targets or operationally validated intervention limits. Future research could extend the proposed framework by incorporating time-varying transmission rates, age-dependent disease dynamics, spatial heterogeneity, and population mobility. More realistic intervention constraints, including vaccine availability, healthcare capac-

ity, implementation delays, and intervention costs, could also be incorporated, together with parameter calibration using epidemiological data, to improve the practical applicability of the proposed control strategy.

A more comprehensive quantitative evaluation, including cumulative infection measures, integrated control effort, tracking error metrics, and sensitivity analysis with respect to epidemiological parameters, remains an important direction for future research.

4. Conclusions

This study developed an adaptive sliding mode control (ASMC) framework for an SVEIHR measles transmission model incorporating vaccination and treatment interventions. The proposed approach integrates reference-based regulation of the vaccinated and infectious populations with a dead-zone adaptive mechanism to adjust the switching gains when the tracking errors exceed a prescribed threshold. The mathematical analysis establishes the epidemiological feasibility of the model through positivity and boundedness of the solutions, while the Lyapunov-based analysis demonstrates exponential convergence of the ideal sliding dynamics when the control saturation constraints are inactive.

Numerical simulations conducted over 200 weeks with an initial population of 10 million individuals show that the peak infectious population decreases from approximately 364,005 individuals in the uncontrolled scenario to 75,900 individuals under ASMC, corresponding to a reduction of 79.15%. At the end of the simulation, the vaccinated population reaches approximately 4.61×10^6 individuals, representing 46.09% of the modeled population. The numerical results also indicate that the adaptive gains remain bounded and the control inputs satisfy their prescribed limits.

However, these findings are obtained under the assumed model structure, epidemiological parameters, prescribed reference trajectories, and control bounds. Therefore, the reported improvements should be interpreted as model-based numerical outcomes rather than direct predictions of intervention effectiveness in real-world settings. Future research may incorporate parameter uncertainty, heterogeneous population structures, time-varying transmission rates, more realistic intervention constraints, and data-driven calibration to improve the practical applicability of the proposed framework.

Acknowledgement

The authors gratefully acknowledge Institut Teknologi Sumatera (ITERA) for the financial support provided through the Skema Penguatan Kelompok Keilmuan Tahun Anggaran 2026 under Contract No. 3641l/DST/IT9.2.1/PT.01.03/2026.

References

[1] N. P. Kondamudi, E. H. Tobin, and J. R. Waymack, "Measles," in *StatPearls [Internet]*, Treasure Island (FL): StatPearls Publishing, 2025. Updated May 5, 2025. https://www.ncbi.nlm.nih.gov/books/NBK448068/.

[2] A. O. Yunus and O. A. Olanrewaju, "Fractional-order modeling of vaccination strategies for measles transmission incorporating immune memory," *Virus Research*, vol. 367, p. 199718, 2026. https://doi.org/10.1016/j.virusres.2026.199718.

[3] World Health Organization, "Measles," 2026. Fact sheet, 15 July 2026. https://www.who.int/news-room/fact-sheets/detail/measles.

[4] D. V. Parums, "A review of the resurgence of measles, a vaccine-preventable disease, as current concerns contrast with past hopes for measles elimination," *Medical Science Monitor*, vol. 30, p. e944436, 2024. https://doi.org/10.12659/MSM.944436.

[5] A. N. M. Ansori, "Measles resurgence in indonesia in 2026: Post-pandemic immunity gaps and emerging public health challenges," *Infectious Diseases and Tropical Medicine*, vol. 12, p. e1828, 2026. https://doi.org/10.32113/idtm_20264_1828.

[6] E. J. Nelwan, "Measles in indonesia: Vaccination coverage and identified challenges," *Acta Medica Indonesiana*, vol. 58, no. 1, pp. 3–4, 2026. https://pubmed.ncbi.nlm.nih.gov/41978293/.

[7] Abadi, M. Fakhruddin, R. Artiono, and B. P. Prawoto, "Measles transmission model with vaccination and hospitalization treatments," *Communication in Biomathematical Sciences*, vol. 3, no. 2, pp. 127–134, 2020. https://doi.org/10.5614/cbms.2020.3.2.4.

[8] A. O. Owolanke, O. K. Ogunbamike, O. J. Peter, and J. O. Agbaje, "A mathematical model for measles transmission with optimal interventions and cost–effectiveness analysis," *Discover Public Health*, vol. 23, no. 1, p. 601, 2026. https://doi.org/10.1186/s12982-026-01932-z.

[9] O. J. Peter, "Modelling measles transmission dynamics and the impact of control strategies on outbreak management," *Journal of Biological Dynamics*, vol. 19, no. 1, p. 2479448, 2025. https://doi.org/10.1080/17513758.2025.2479448.

[10] D. Suhika, R. Saragih, and D. Handayani, "Application of nonlinear robust sliding mode control on mathematical model for spreading of covid-19," in *AIP Conference Proceedings*, vol. 3095, p. 050001, AIP Publishing, 2024. https://doi.org/10.1063/5.0205191.

[11] H. Wen, Z. Liang, H. Zhou, X. Li, B. Yao, Z. Mao, and L. Lian, "Adaptive sliding mode control for unknown uncertain non-linear systems with variable coefficients and disturbances," *Communications in Nonlinear Science and Numerical Simulation*, vol. 121, p. 107225, 2023. https://doi.org/10.1016/j.cnsns.2023.107225.

[12] D. Suhika, R. Saragih, D. Handayani, and M. Apri, "Sliding mode control with stochastic modeling and mobility interaction for managing epidemic spread in high-population regions," *Parasite Epidemiology and Control*, vol. 30, p. e00439, 2025. https://doi.org/10.1016/j.parepi.2025.e00439.

[13] X. Chen, C. Xiang, and Y. Yang, "Sliding mode control of the susceptible-exposed-asymptomatic-infected-recovered model with vaccination," *Mathematical Methods in the Applied Sciences*, vol. 48, no. 3, pp. 3936–3955, 2025. https://doi.org/10.1002/mma.10526.

[14] M. Ariyanatchi and G. M. Vijayalakshmi, "Nonlinear robust adaptive sliding mode control strategies involve a fractional ordered approach to reducing dengue vectors," *Results in Control and Optimization*, vol. 14, p. 100406, 2024. https://doi.org/10.1016/j.rico.2024.100406.

[15] A. Boonyaprapasom, S. Natsupakpong, P. S. Ngiumsunthorn, and K. Thung-od, "Fractional order sliding mode control for vaccination in epidemic systems," in *2017 2nd International Conference on Control and Robotics Engineering (ICCRE)*, (Bangkok, Thailand), pp. 145–149, IEEE, 2017. https://doi.org/10.1109/ICCRE.2017.7935059.

[16] D. Suhika, R. Saragih, D. Handayani, and M. Apri, "Adaptive sliding mode control under uncertainty for a stochastic epidemic model with mobility," in *2025 25th International Conference on Control, Automation and Systems (ICCAS)*, (Incheon, Korea, Republic of), pp. 1189–1194, IEEE, 2025. https://doi.org/10.23919/ICCAS66577.2025.11301158.

[17] D. Suhika, R. Saragih, D. Handayani, and M. Apri, "A vaccination and isolation strategy based on an adaptive sliding mode control design for the covid-19 virus (omicron variant) in jakarta, indonesia," *Communication in Biomathematical Sciences*, vol. 8, no. 1, pp. 19–41, 2025. https://doi.org/10.5614/cbms.2025.8.1.2.

[18] D. Aldila, A. H. Hassan, C. W. Chukwu, S. Y. Tchoumi, and M. H. N. Aziz, "Evaluating vaccination and quarantine for measles intervention strategy in jakarta, indonesia through mathematical modeling," *Partial Differential Equations in Applied Mathematics*, vol. 14, p. 101191, 2025. https://doi.org/10.1016/j.padiff.2025.101191.

[19] A. Deka, T. Mahato, and S. Bhattacharyya, "A mathematical model for distributed waning of vaccine-derived immunity: Characterizing dynamical impact on measles elimination," *Franklin Open*, vol. 9, p. 100174, 2024. https://doi.org/10.1016/j.fraope.2024.100174.